World's First Fully Rated Direct ac/ac MMC for Variable-Speed Pumped-Storage Hydropower Plants

Alexandre Christe, *Member, IEEE*, Alexander Faulstich, Michail Vasiladiotis, *Senior Member, IEEE*, and Peter Steinmann

***Abstract*—This article presents in-depth insights about the development and successful introduction in the field of the first direct ac/ac modular multilevel converter (MMC) as static frequency converter (SFC) for a converter-fed synchronous machine (CFSM) variable-speed pumped-storage hydropower plants (PSHPs). Thanks to a fully rated SFC, the grid dynamics are completely decoupled from the machine dynamics, enabling a straightforward variable-speed operation with high torque over the entire speed range, starting from standstill. Over the whole speed range, the synchronous machine (SM) can be controlled at unity power factor, resulting in a smaller machine compared to a fixed-speed PSHP. The pump start without water blow-down in the turbine chamber means faster and simpler mode transition between turbine and pump operation. Thanks to the wide variable-speed range, the hydraulic efficiency of the turbine can be finely optimized. This results in increased partial-load efficiency and never seen cycle efficiency numbers. The possibility to provide balance energy also in pump operation offers great advantages to the plant's owner. A comprehensive measurement set acquired during the commissioning of the Malta Oberstufe plant in Austria asserts the suitability of a direct ac/ac MMC as SFC for a CFSM variable-speed PSHP.**

***Index Terms*—AC–AC converters, energy storage (ES), hydroelectric power generation, modular multilevel converters (MMCs).**

I. Introduction

DRIVEN by the massive introduction of renewable energy sources (RESs) as replacement for traditional synchronous generation, such as carbon and nuclear, the electrical grid is undergoing a profound transformation toward being the backbone of the entire energy system of the future. Besides these expansions, numerous reinforcement measures are being taken for strengthening the grid. In addition to the topics of virtual inertia and fast frequency response [1], [2], large-scale energy storage (ES) solutions are required for peak shaving and annual compensation of the intermittent nature of RESs.

Among the available solutions, pumped-storage hydropower (PSH) constitutes a well-established one. For many decades, fixed-speed units [cf. Fig. 1(a)] have been used. Conventional fixed-speed units have no flexibility in pump mode and complex start procedure in pump operation [3], while ternary set units achieve controllability in pump mode by using a separate turbine and pump on the same mechanical shaft with a clutch employing a hydraulic short circuit, resulting in a much more complex hydraulic and mechanical design [4]. There is a trend nowadays to replace (a part of) the conventional fixed-speed units with variable-speed ones in order to gain flexibility. On the grid side, balance energy also in pump mode is a major advantage as the active power flow can be controlled and adjusted. It also opens the door for frequency control in pump mode. This makes it a natural complement for large-scale RESs [5], [6]. In addition, enhanced grid ancillary services capabilities are provided to the plant owners, which see additional revenue schemes and streams.

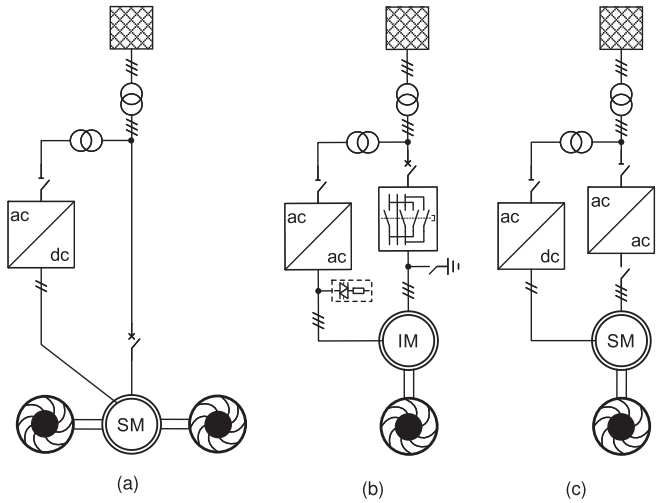

Fig. 1. Possible PSHP configurations: (a) ternary set with machine breaker and distinct pump and turbine, (b) DFIM with either direct or indirect ac/ac SFC, machine breaker, pole reversing switch and thyristor crowbar and (c) CFSM with either direct or indirect ac/ac SFC. Note that additional switches, e.g., grounding switches for maintenance, or charging circuits, are not shown for sake of clarity.

Manuscript received 28 March 2022; revised 19 July 2022; accepted 29 August 2022. Date of publication 13 September 2022; date of current version 17 February 2023. *(Corresponding author: Alexandre Christe.)*

The authors are with the Grid and Power Quality Solutions, Hitachi Energy Switzerland Ltd., 8050 Turgi, Switzerland (e-mail: alexandre.christe@hitachienergy.com; alexander.faulstich@hitachienergy.com; michail.vasiladiotis@hitachienergy.com; peter.steinmann@hitachienergy.com).

Color versions of one or more figures in this article are available at https://doi.org/10.1109/TIE.2022.3204858.

Digital Object Identifier 10.1109/TIE.2022.3204858

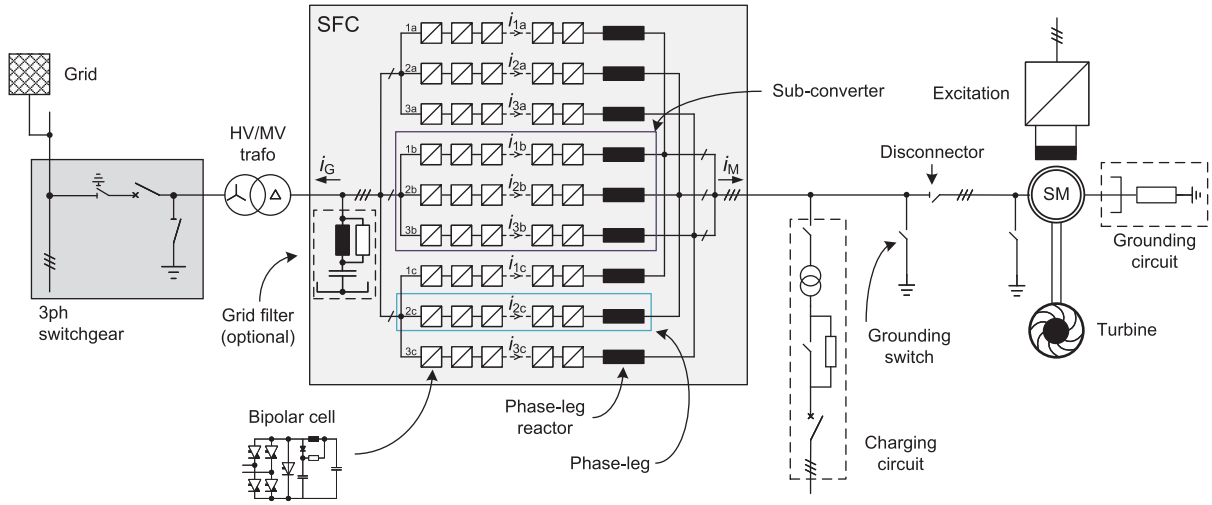

Fig. 2. Single-line diagram for a CFSM PSHP with a direct ac/ac MMC as SFC.

Two variable-speed solutions are available, both requiring a SFC: 1) doubly-fed induction machine (DFIM) [cf. Fig. 1(b)] and 2) CFSM [cf. Fig. 1(c)]. Some important differences exist between both solutions, and no real consensus regarding which shall or could be the preferred solution is achieved [7]. The business model and head variation might finally dictate which is the preferred solution. In any case, variable-speed operation is particularly advantageous [8]. It enables higher head variation, reduces vibrations, and cavitations and results in higher hydraulic efficiency, especially at partial load. For a DFIM, the SFC is rated for a fraction of the machine nominal power and the induction machine (IM) has three-phase connections both to the stator and rotor (through slip rings), which leads to a substantial rotor mass increase (approximately 30% higher weight for a DFIM compared to a SM [9]). For a CFSM, the SFC is fully rated and a conventional (separately excited) SM is connected. In case a converter bypass for turbine operation is not foreseen, which is beneficial in order to fully leverage the presence of the SFC, the nominal frequency of the SM becomes a design parameter as well. Also, static synchronous compensator (STATCOM) operation with machine at standstill, or potentially under maintenance, is available.

This article is focused on the CFSM solution. Compared to a DFIM, it offers a faster and simplified start-up procedure in pump mode, due to the higher starting torque and no need for grid synchronization. Also, the variable-speed range is not constrained by the maximum machine slip and rotor voltage. The SFC technology for DFIM evolved from cycloconverter [10] to three-level voltage-source converter (VSC) [11], [12]. Until recently, CFSMs were facing challenges due to inadequate converter terminal voltage (compared to typical machine terminal voltages), requiring dv/dt filters and transformers on the machine side, making the pump start difficult due to transformer saturation, as in the world's first CFSM PSHP Grimsel 2, which was commissioned in 2013 and with a three-level VSC SFC rated 100 MVA [13] or multilevel monolithic VSCs [14], which may still require dv/dt filters, series-connected semiconductors, potential additional passive components for mitigating circulating currents between parallel converters and higher losses compared to MMCs. Indirect MMC has only been considered [15], [16], [17], but so far to our best knowledge none has been commissioned. With a direct ac/ac MMC, the SM is directly connected to a SFC with a very low harmonic content, which leads to the following simplified single-line diagram (cf. Fig. 2). In [18], it is reported that for fast transition from turbine to pump mode the direct ac/ac MMC is the best candidate, since it does not lead to converter oversizing. This current overload capability is also reported in [19], leading to higher achievable torque at low machine speed. SFCs with a direct ac/ac MMC have already a proven track record in the field with rail interties [20], [21]. In [22], the foundations for this game changer solution were laid. The basic design and functioning principles were introduced. In this work, insights from the first introduction in the field of such a converter will be presented.

This article is organized as follows. First, system design aspects, i.e., how to size the converter, will be discussed. Then, a few words about the control and protection (C&P) of such a plant will be provided. Moving forward, results from the recently commissioned first plant [23] will be presented. Finally, a conclusion will summarize the experience gained in this journey.

II. System Design

The single-line diagram of a direct ac/ac MMC for a CFSM PSHP is given in Fig. 2. A standard step-down Y/Δ transformer is adjusting the SFC voltage level to the upstream grid. The SM is coupled to the SFC with just a disconnector, which is operated at no load nor voltage. The charging circuit is used to precharge the converter prior to transformer magnetization for a smooth grid synchronization. A recording of the same cell charging and discharging is available in [22], Fig. 13]. The grounding switches are there for securing the installation

during maintenance mainly. An harmonic filter may be required depending on site conditions and interconnection requirements. One possible way of grounding the SFC and the SM is shown on the figure. Same applies to the charging circuit, which can be placed on either SFC side.

The SFC is made of nine phase-legs (or branches), each of which consists of a series-connection of bipolar (full bridge) cells and a phase-leg reactor. The cell is based on reverse-conducting insulated gate controlled thyristors (RC-IGCTs) and contains a bypass thyristor to discharge the capacitor and provide a stable short-circuit path in case of component failure. Please refer to Fig. 2 for a cell circuit diagram. Details regarding the cell's characteristics, along with its robustness can be found in [24].

For a direct ac/ac MMC, the voltage u_{xy} and current i_{xy} of one phase-leg with $x \in \{1,2,3\}$ and $y \in \{A,B,C\}$ are defined as

$$u_{xy} = u_{\text{conv,G},y} - u_{\text{conv,M},x} + u_{\text{CM}} + u_{\text{circ},xy} \tag{1a}$$

$$i_{xy} = -\frac{i_{\text{G},y}}{3} + \frac{i_{\text{M},x}}{3} + i_{\text{circ},xy}. \tag{1b}$$

where $u_{\text{conv,G},y}$ is the converter voltage towards the grid in phase y, $u_{\text{conv,M},x}$ the converter voltage toward the machine in phase x, u_{CM} the common mode voltage (CMV), $u_{\text{circ},xy}$ the circulating voltage driving the circulating current (CC) $i_{\text{circ},xy}$, $i_{\text{G},y}$ the grid current in phase y and $i_{\text{M},x}$ the machine side current in phase x. They comprise at least terms at the grid and machine frequencies. By observing Fig. 2, the grid and machine side currents (i_{G} and i_{M}) are naturally equally split among the three phase-legs connected to the same ac terminal, hence the $1/3$ factors in (1). Other current allocations are also possible depending on the operating point [25], [26], [27].

The CMV u_{CM} is the voltage appearing between the SM and the transformer neutral points. This voltage is typically controlled to reduce the peak value of the phase-leg voltages, thus reducing the number of cells or equivalently increasing the modulation index and therefore the available power. The CMV injection is defined as

$$u_{\text{CM}} = -\frac{\max(u_{\text{conv,G,ABC}}) + \min(u_{\text{conv,G,ABC}})}{2} + \begin{cases} 0 & \left|\frac{f_{\text{M}}}{f_{\text{G}}}\right| < \frac{2}{5} \\ \frac{\max(u_{\text{conv,M,123}}) + \min(u_{\text{conv,M,123}})}{2} & \left|\frac{f_{\text{M}}}{f_{\text{G}}}\right| \geq \frac{2}{5} \end{cases} \tag{2}$$

assuming the min/max method is selected [28]. In the low speed region, CMV is not required due to the also low machine voltage. At the same time, around $|f_{\text{M}}| = f_{\text{G}}/3$ (and for potentially additional triplen harmonics like $f_{\text{G}}/9$, $f_{\text{G}}/15$, etc., depending on the spectrum of the CMV injection method) an additional issue exists: the CMV would interact with the fundamental frequency grid currents, thus giving rise to dc energy terms destabilizing the phase-leg voltage balancing. For the aforementioned reasons, the control system is injecting CMV according to (2). Finally, by using an appropriate grounding scheme and owing the parasitic capacitances ratio between the SM stator and the transformer (by an order of magnitude larger on the SM), most of the CMV, which is to a large extent imposed by control to increase the modulation index, is appearing at the transformer's terminals. Therefore, the impact of CMV on the machine isolation is negligible.

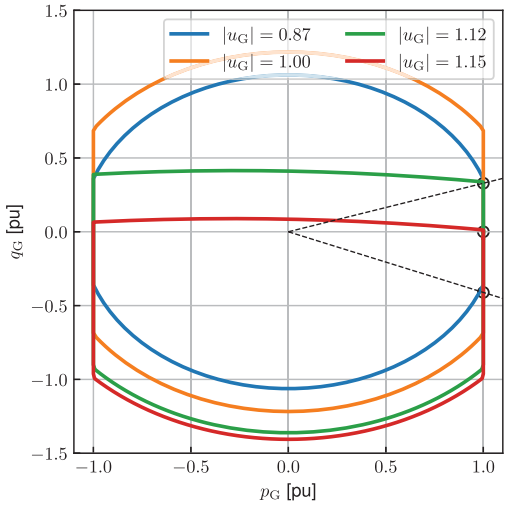

Fig. 3. Example of pq diagrams at the PCC for different voltages, where dashed lines correspond to specific power factors.

The controllable voltages u_{circ} drive respective CCs i_{circ}, which are internal (proprietary) MMCs quantities that do not affect any SFC terminal. Their purpose is to perform the energy balancing control, i.e., the average capacitor voltages shall be equal among all nine converter phase-legs. Extensive technical details about the energy balancing control of a direct ac/ac MMC fall out of the scope of this article. The interested readers are referred to the already available nonexhaustive literature on the topic [25], [29], [30], [31].

A. Grid-Side PQ Capability

The required SFC's active (p_{G}) and reactive (q_{G}) power capability at the point of common coupling (PCC) is specified by the customer requirements as well as the grid code relevant for the plant. An example of such a pq diagram is shown in Fig. 3 for a range of PCC voltages. It is clear that the SFC offers all possible operation combinations, including pump/turbine active power flows as well as overexcited/underexcited power factors on the grid side. Due to the direct ac/ac MMC topology, at low machine voltage, i.e., low machine speed, there is some additional voltage and current margin which could be used to further expand the pq diagram for more reactive power on the grid side.

B. Further System and Design Aspects

Low-frequency operation is only a concern in pump mode, where the SFC delivers active power to the turbine, as in turbine operation the machine run-up is entirely done by water, with the SFC contributing only minimally to maintain a constant speed ramp. Contrary to a SFC based on an indirect MMC with unipolar cells [32], the machine run-up in pump mode is seamless. This can be observed in Fig. 4, where a quadratic load

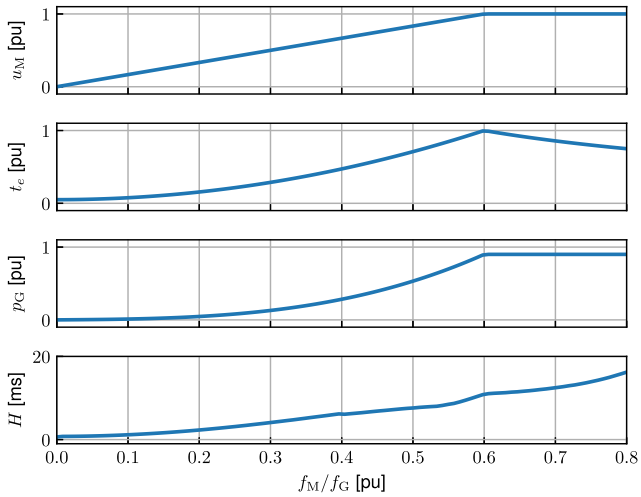

Fig. 4. Typical direct ac/ac MMC stored energy requirement[1] over the whole speed range, with a quadratic load torque ($k_0 = 5\%$) and constant power factors of $\cos\phi_G = 0.9$ on the grid side and $\cos\phi_M = 1$ on the machine side. Note that the CMV injection on the machine side is enabled for $|f_M/f_G| \geq 2/5$.

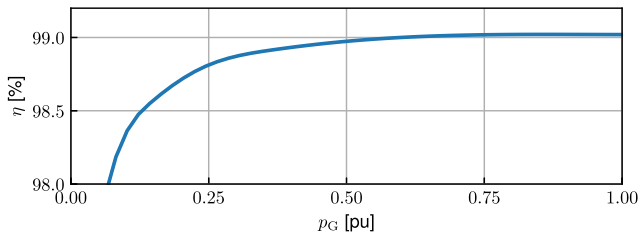

Fig. 5. Total converter cell efficiency for variable speed operation with a quadratic load torque profile as in Fig. 4.

torque, typical for pump operation, is defined as

$$t_e = k_0 + (1 - k_0) f_M^2 \tag{3}$$

and is followed by constant power in the field weakening region.

Typically, a direct ac/ac MMC using RC-IGCT devices leads to very high total converter cell efficiencies. The latter includes power semiconductor, clamp circuit, cell capacitor, and low power electronics (gate drivers, cell power supplies) losses. Assuming variable speed operation with a quadratic load torque profile, the cell efficiency is shown in Fig. 5. It is noted that the resulting total converter cell efficiency is also highly depending on the chosen switching frequency, which is in turn depending on the required number of cells for a specific design as well as the grid harmonic performance requirements. For details on the resulting system-level power losses, the reader is referred to [22]. As indication, the average hydraulic efficiency gains compared to the previously installed fixed-speed SM amount to 7% to 9% in turbine mode and 6% to 22% in pump mode in the commissioned plant [23].

Since the SM is not directly connected to the grid, it can be designed for $\cos\phi_M = 1$, as opposed to conventional hydro generator designs with $\cos\phi_M = 0.9$. This results in comfortable savings in machine weight, size, and cost, which can reach up to 18% according to [34]. The variable-speed range depends on the physical configuration of the plant and is mainly depending on the altitude difference in the upper lake. From the converter side, the only barrier is the synchronous operation (equal grid and machine frequencies). With a CFSM, the theoretically usable speed range starts from standstill. In practice, mechanical resonances and cavitation might appear at low speeds. At the other extremity, the operation at close or equal frequencies comes with too many constraints for a direct ac/ac MMC. If the system is fully decoupled through the use of CMV and CCs [25], [35], it results in either converter oversizing or reduced power transfer capability and at the same time increased losses. If the reactive power flow is to be matched on both sides [25], [26], the ability to control it on the grid side is sacrificed. Consequently, a reasonable variable-speed range, where the turbine can be exploited without compromises is

$$\left|\frac{f_M}{f_G}\right| \in [0.3, 0.8]. \tag{4}$$

Another aspect relates to dv/dt and over-voltages. These might occur in steady-state operation, due to the SFC voltage resolution and harmonics, and might be further amplified in case the machine is connected with long cables, due to their capacitance. They may also occur due to transient operation, e.g., due to a too high current gradient during a load rejection. For these reasons, damping resistors can be placed in parallel to the phase-leg reactors [23], ensuring smooth waveforms for the electrical machine.

III. Control and Protection

The overall C&P's overview for a PSHP is shown in Fig. 6. It features different control systems from different subsuppliers, which are running at different time scales. The scope of this article is limited to the SFC. Consequently, the other systems will not be described.

The SFC's C&P system is made of three entities: 1) the open-loop and sequence control, which is dedicated to the interface with other control systems, the actuation of various switches and breakers, the cooling system control, and other non time critical functions, 2) the closed-loop control, which performs all the time critical (closed-loop) control actions, and 3) the converter protection, which monitors physical devices within its scope.

A. Open-Loop and Sequence Control

The open-loop and sequence control handles the communication between the SFC and the other control systems. In particular, it includes set-points exchange with the governor control and the excitation control. Other executed slow control tasks worth mentioning are the transformer tap-changer position and cooling flow control.

It is also performing sequences between the various states of the SFC, as shown in Fig. 7. The five states are described as follows:

[1]Where $H = 9\Delta E_{PhL}^{max}/S_n \cdot 1e3$ in [ms] or [kJ/MVA] (see [33]).

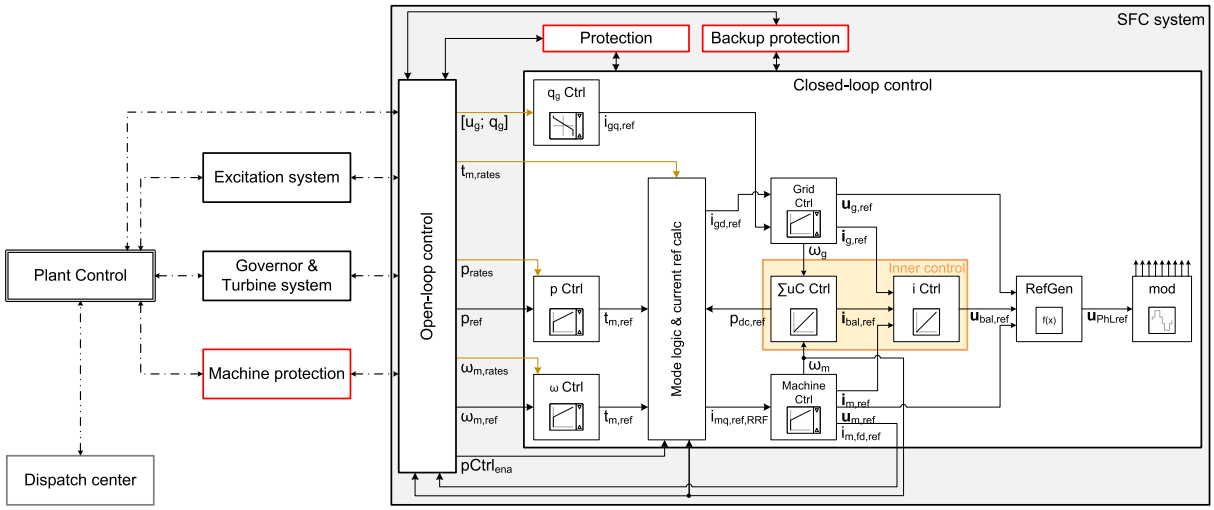

Fig. 6. Control overview at the plant level. The governor receives set-points from the remote dispatch center and distributes them to the various control systems of the PSHP. Most of the control is then performed by the turbine controller and the SFC's controller.

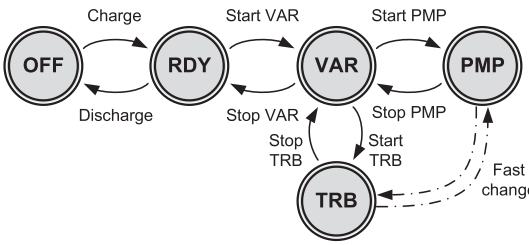

Fig. 7. SFC states and possible transitions performed by the open-loop control.

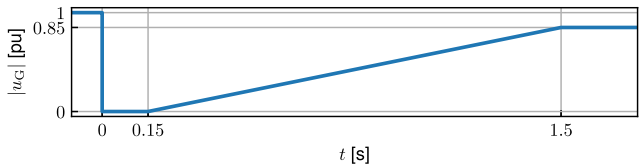

Fig. 8. Voltage curve for LVRT as specified for a generator of Type D in the Austrian grid code [39]. The SFC is not allowed to block the pulses as long as the grid voltage is above or equal to the curve. For HVRT there is usually another curve.

OFF The SFC is de-energized, the grid-side breaker is open and the machine disconnector is open.

RDY The SFC is charged, connected to the grid and ready to start operation and the machine disconnector is closed.

VAR The SFC is operated as a STATCOM, exchanging reactive power with the grid, while the machine is at standstill.

PMP The SFC is absorbing power from the grid and delivering active power to the SM in order to pump water up.

TRB The SFC is delivering active power to the grid and absorbing active power from the SM as the water goes down.

B. Closed-Loop Control

The SFC's closed-loop control aims at controlling either the speed or the power of the SM and the reactive power exchange toward the ac grid, which are shown on the left side of the "Closed-loop control" in Fig. 6. At low speed, the SFC always operates in speed control mode, to bring the machine up to the variable speed range or down to standstill, while in normal operation the SFC operates in power control mode (cf. mode logic). In turbine mode, the governor controls the guide vanes opening and performs speed control, while in pump mode the turbine characteristic does not allow for much degree of freedom. This provides a very stable operation on the machine side regardless of the little disturbances that might occur on the grid side. Besides that, several additional control layers are required, covering the grid-side control (based on the voltage-oriented control principle [36]), machine-side control (based on the field-oriented control principle [37], [38]), MMC inner control [25], [29], [30], [31], phase-leg voltage references assembly and the modulator [22], which translates the phase-leg voltage references into firing pulses for the semiconductor devices. Worth highlighting, the dynamics on the machine-side are slowed-down compared to the SFC's capabilities via several rate limiters (for the speed, electrical torque, and active power) to avoid mechanical instabilities or unacceptable stresses. Most of the grid disturbances are buffered by the SFC, and the SM is always operated at unity power factor.

Grid faults are undesired, nonetheless existing events in a grid. Due to historical reasons, the protection relays are isolating the faulty part of the grid based on the detection of over-currents. This means any grid code specifies that a converter shall inject reactive current during faults. At the same time, this current injection results in a voltage rise nearby the converter. In its most simple form, the converter shall react to voltage dips by injecting reactive currents, so that the amplitude of the positive-sequence PCC voltage is boosted and the negative-sequence one reduced. The minimum voltage to ride-through depends on the plant's power. An example is provided in Fig. 8.

TABLE I
MALTA PSHP PARAMETERS FOR A SINGLE CFSM DIRECT AC/AC MMC

$P_{\min}..P_{\max}$	8..80 MW	$S_{\mathrm{b,MMC}}/S_{\mathrm{SC}}$	89/300 MVA
$S_{\mathrm{b,G}}$	89 MVA	$S_{\mathrm{b,M}}$	80 MVA
$U_{\mathrm{b,G,pri}}/U_{\mathrm{b,G,sec}}$	110/18.7 kV	$U_{\mathrm{b,M}}$	18 kV
f_{G}	50 Hz	$f_{\mathrm{M,min}}..f_{\mathrm{M,max}}$	17..40 Hz

C. Protection

Protective measures are taken for a safe and reliable operation of the SFC in the plant. The main and backup protection are performed on independent controllers operating separate tripping coils. The protection settings are coordinated with the customer and network operator on a project specific basis.

IV. Development and Verification

A project, from tender to commissioning, goes through a multistep process. In the tender phase, an in-house system design optimization tool [40] determines the best suited design, accounting simultaneously for various well-known multiobjective optimization criteria such as volume, cost, and efficiency, but also project specific aspects, such as limits from the hydraulics, grid compliance based on available grid data, weighted efficiency over the whole operation range, etc.

Before its deployment to site, the control and protection software undergoes a thorough two-step verification process. First, each control concept or functionality is tested in an electromagnetic transients (EMT) simulation environment, which accurately reproduces the various delays from the real hardware. Second, the control software is verified on a real-time simulator (RTS), where an exact control hardware replica from site is being verified. The ac grid, SFC, SM, excitation system and turbine are modeled in a commercial hardware-in-the-loop (HIL) system.

V. Results

The world's first direct ac/ac MMC for CFSM PSHP has recently been successfully put into operation in Malta Oberstufe (Austria). Since mid-January 2022, both units have been handed over to the customer for commercial operation.

There are two 80 MW CFSM units, which replace two fixed-speed 60 MW units. Details about the plant are available in [23]. The specifications for a single unit are listed in Table I, alongside with the turbine diagram provided in Fig. 9. Please note that these are site specific and result from an optimization from the turbine manufacturer that accounts for the height difference between the two lakes in addition to the unit's power. A big advantage of the CFSM is that the turbine operation can be optimized freely without any variable-speed range constraint from the SFC. Such a wide variable-speed range would never have been possible with a DFIM, and the turbine's efficiency would have been compromised.

During commissioning, a large number of tests to verify the behavior and the coordination between the various C&P systems have been performed, along with efficiency, heat run and grid

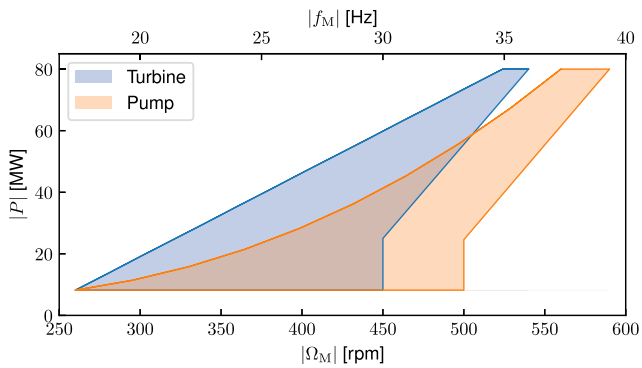

Fig. 9. Turbine usable range for the Malta PSHP. The upper extreme of the turbine characteristic is only reached a few days per year, when the upper lake is at its highest level.

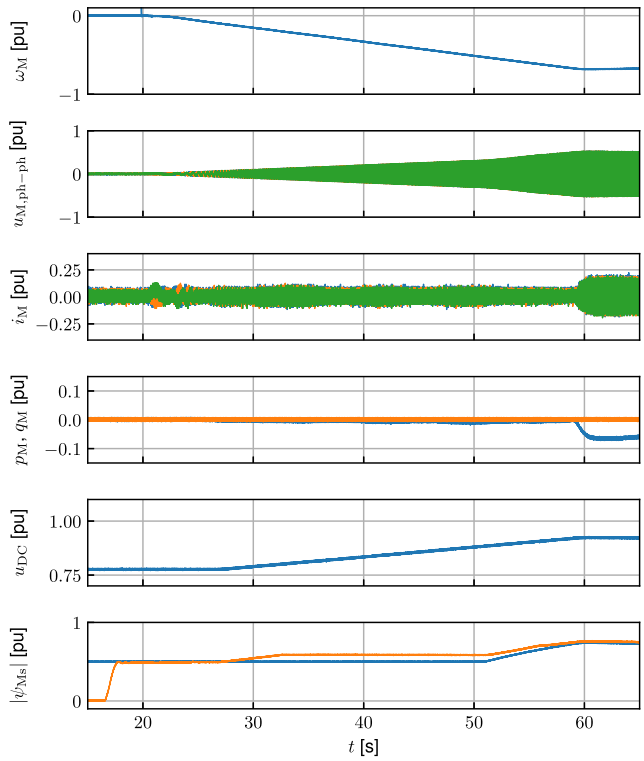

Fig. 10. Start in turbine mode recorded on site during commissioning.

acceptance tests. From this large set of data, the following real-world measurements were selected: 1) start sequence in turbine mode, 2) start sequence in pump mode, 3) stop sequence in pump mode, 4) power ramp in turbine mode, 5) transition from turbine to pump mode, and 6) grid earth fault. All the measurements have been acquired either by direct recording of signals inside the control platform or by oscilloscope trending.

During turbine start, as shown in Fig. 10, the SM is accelerated from the water, and no active power is drawn from the grid to start-up the machine. The SFC regulates the speed ramp according to the speed reference received from the governor control. Once in the operational speed range, active power is delivered to the grid.

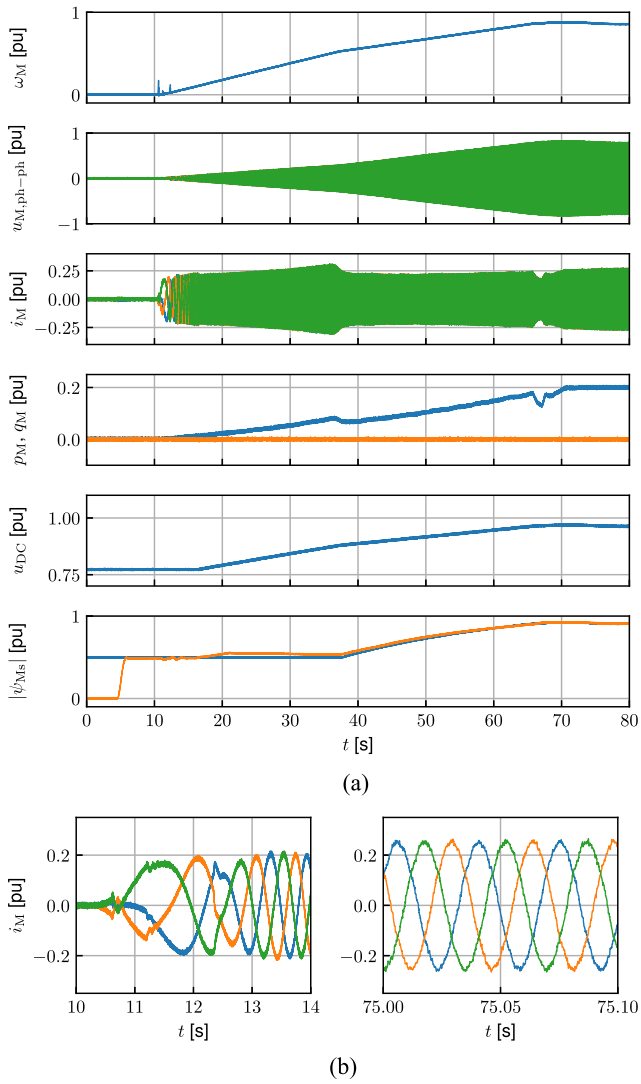

Fig. 11. Wet start in pump mode recorded on site during commissioning: (a) long trending over 80 s and (b) zoomed machine-side currents at the very start and very end of the recording.

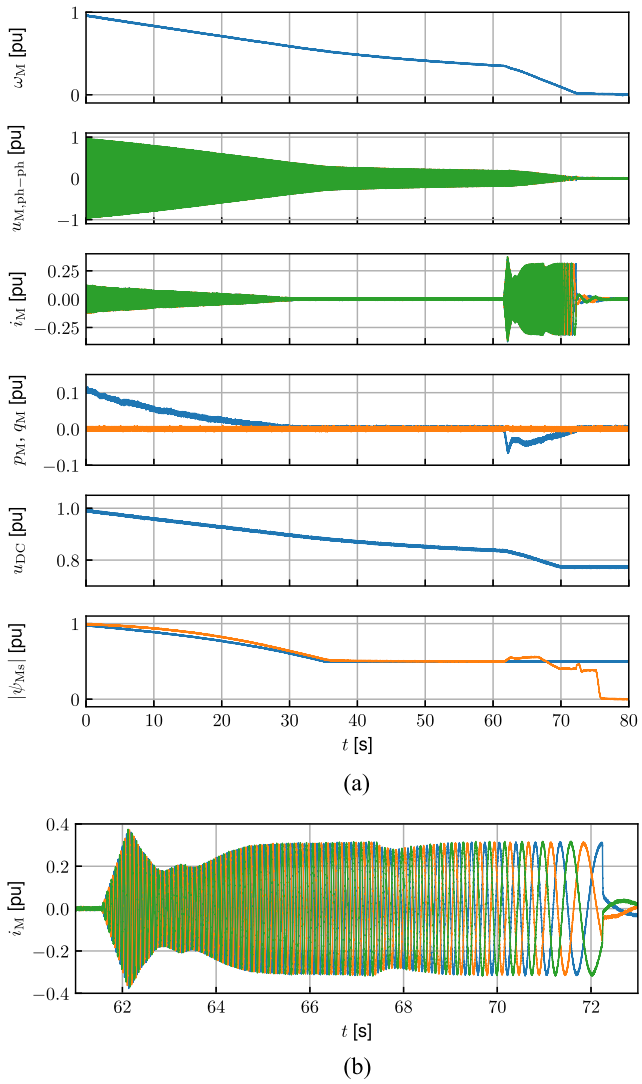

Fig. 12. Stop sequence in pump mode recorded on site during commissioning: (a) long trending over 80 s and (b) zoomed machine-side currents during the end of the braking sequence.

During pump start, as shown in Fig. 11, first pressure is built-up in the turbine chamber with the main valve closed until $t = 36$ s. In this way, cavitation can be greatly avoided when opening the main valve and starting to pump water up thanks to a sufficient hydraulic pressure. At $t = 65$ s, the SFC changes from speed to power control. The turbine governor does not really perform a speed control, since the guide vanes are only opened proportionally to the turbine speed. Assuming that the converter is in STATCOM mode prior to the pump start, it takes only 25 s before reaching the minimum speed for starting pump operation (in this case 0.52 pu). It can be observed that the currents are slightly distorted at the beginning of the ramp in Fig. 11(b). These disturbances coincide with the encoder vibrations which can be seen in the speed measurement. The frequency ramp is 0.02 pu/s.

Fig. 12 presents the braking sequence in pump mode. As it can be observed, the electrical braking is completely interrupted between $t = 30$ s to $t = 62$ s, during which the main valve is closed. This is a slow hydromechanical process. After that, the SFC receives the command to bring the machine to standstill with a fast speed gradient of 0.044 pu/s. Following this, the machine excitation is switched-OFF to avoid any damage to the excitation brushes.

In Fig. 13, a 10% power ramp down performed by the turbine governor around 80% speed in turbine mode is shown. The SFC is operated in power control mode, while the turbine governor controls the speed of the turbine through an action on the angle of the guide vanes. The optimal operating point (ω_M, p_M) leads to a slight speed adjustment. Only three phase-leg capacitor voltage sums are recorded in Fig. 13(b). The multifrequency harmonic content of these voltages and the phase-leg currents is manifest.

In Fig. 14, the transition from turbine to pump mode is shown. As it can be seen, the transition is performed in less than 100 s. Between $t = 25$ s to $t = 45$ s, is the machine actively braked from the SFC. The waiting time at zero speed that follows is due to how the sequence control is performed on the plant

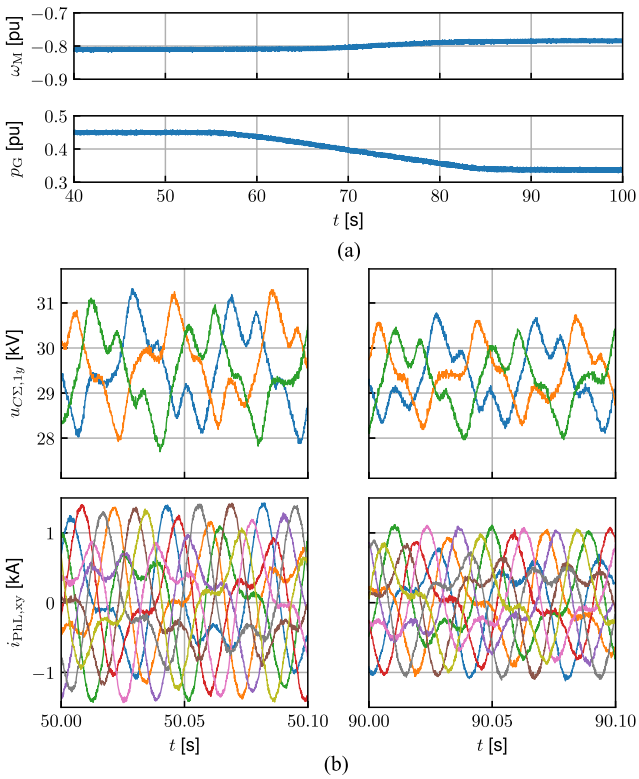

Fig. 13. Power ramp in turbine mode from 40 to 30 MW recorded on site during commissioning: (a) long trending over 60 s and (b) zoomed steady-state operation at 40 and 30 MW, respectively.

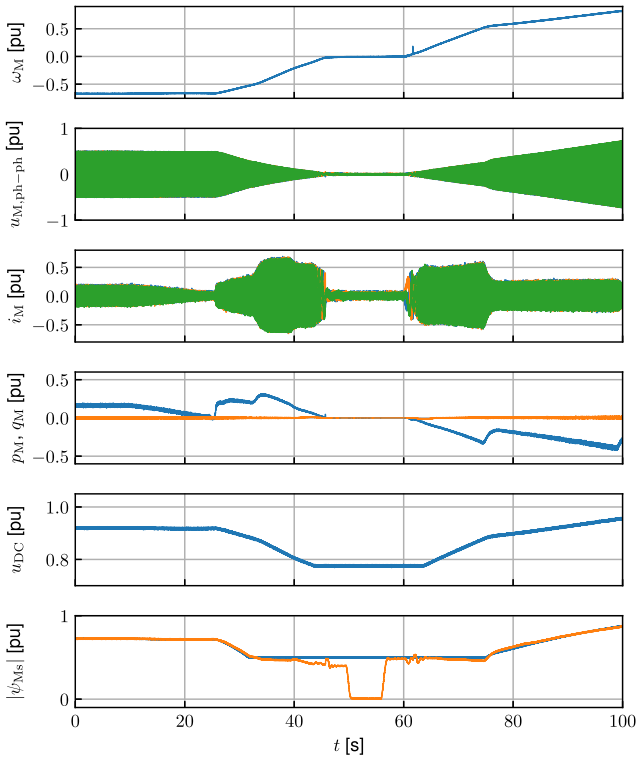

Fig. 14. Transition from turbine to pump mode recorded on site during commissioning.

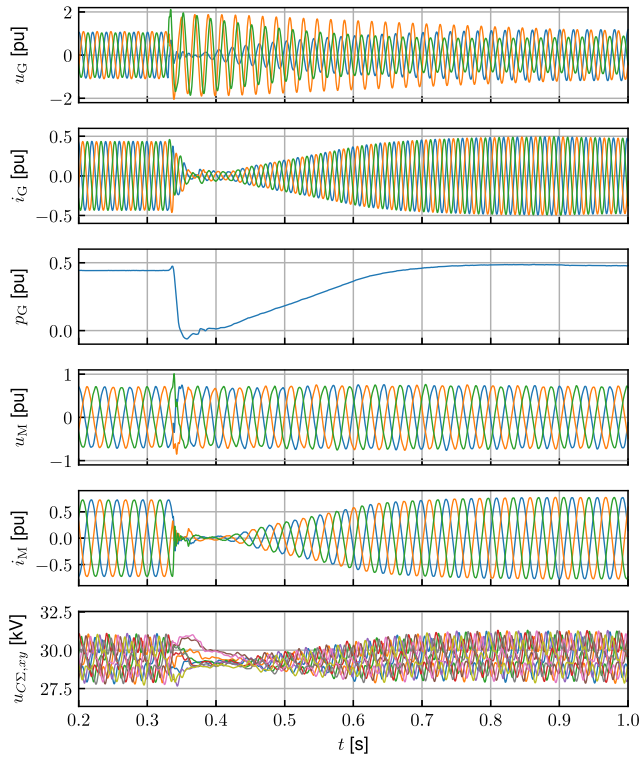

Fig. 15. Grid earth fault in turbine operation near the powerhouse recorded on site during commercial operation, which manifests itself with a significant zero-sequence voltage on the transformer's primary side.

control side. There is no restriction from the SFC not to start pump operation right away. Note that the excitation current is brought down to zero to avoid thermal issues on the brushes due to the long time spent at $\omega_M = 0$. Then, at $t = 55$ s, the command to start pump operation is received. Note that faster transitions as reported in [18] and [41] are not possible in Malta due to the limited maximum hydraulic pressure.

During the recordings presented in Figs. 11–14, the SM is successfully maintained at unity power factor over the whole speed range. At low machine speed, the converter virtual dc voltage is reduced, leading to reduced losses and improved harmonic performance.

A grid earth fault at the vicinity of the powerhouse was recorded in Fig. 15. As soon as a grid voltage dip is detected, the machine power is quickly brought down to zero to limit the risk of a converter trip due to cell over-voltage. Since a grid earth fault has no impact on the SFC and no special requirements for suitable fault current injection are specified in the grid code, the operating resumes soon after. At the time of writing, this is the only grid fault recorded on site since the SFCs are in operation.

VI. Conclusion

This article presented the successful introduction in the field of a game changer solution for CFSM PSHP with a direct ac/ac MMC as SFC.

On the system design side, besides system description, it was shown how a typical pq diagram looks like for different

PCC voltages. The consideration of the load profile during machine run-up was translated in energy storage requirement. The cell hardware efficiency was then presented for two illustrative power factors. It exceeds 99% above 0.7 pu, meaning an electrical system efficiency of more than 98.5% is achievable.

The suitability of the C&P system provides very good dynamics and control performance to the whole CFSM PSHP in all scenarios, including fault ride-through (FRT). Compared to a fixed-speed unit, the differences are very important. The load steps are very smooth without mechanical oscillations and the risk for cavitations is much reduced, which is an advantage regarding maintenance needs and components wear. The controllability in pump operation is a huge benefit for the plant owner, which gains balance energy and frequency control in pump operation.

The measurements recorded on site during commissioning or commercial operation support what is known by the authors as the first full-scale direct ac/ac MMC in commercial operation. All relevant scenarios have been covered. The SFC performs as expected and the plant runs to the satisfaction of the owner.

Acknowledgment

The authors would like to thank B. Buchmann, S. Herold, D. Wu, Shanmugam V., C. Häderli, M. Kläusler, G. Beanato, and J. Steinke for their contributions at various levels and stages during the execution of the project.

References

[1] A. Tuckey and S. Round, "Grid-forming inverters for grid-connected microgrids: Developing "good citizens" to ensure the continued flow of stable, reliable power," *IEEE Electrific. Mag.*, vol. 10, no. 1, pp. 39–51, Mar. 2022, doi: 10.1109/mele.2021.3139172.

[2] M. Lombardo, M. Asoodar, J.-P. Hasler, and J. Kheir, "Synthetic inertia using synchronous machines interfaced with power electronic converters," in *Proc. IEEE 12th Energy Convers. Congr. Expo. - Asia*, 2021, pp. 2016–2021, doi: 10.1109/ECCE-Asia49820.2021.9479289.

[3] P. G. Brown and G. W. Otte, "Electrical design considerations in pumped storage hydro plants," *Elect. Eng.*, vol. 82, no. 11, pp. 654–660, 1963, doi: 10.1109/EE.1963.6539709.

[4] J. Feltes et al., "Modeling ternary pumped storage units," Oct. 2013. [Online]. Available: https://www.osti.gov/biblio/1098020, doi: 10.2172/1098020.

[5] M. Mosadeghy, T. K. Saha, and R. Yan, "Increasing wind capacity value in Tasmania using wind and hydro power coordination," in *Proc. IEEE Power Energy Soc. Gen. Meeting*, 2013, pp. 1–5, doi: 10.1109/pesmg.2013.6672585.

[6] A. A. S. de la Nieta, J. Contreras, J. I. Munoz, and J. P. S. Catalao, "Optimal wind reversible hydro offering strategies for midterm planning," *IEEE Trans. Sustain. Energy*, vol. 6, no. 4, pp. 1356–1366, Oct. 2015, doi: 10.1109/tste.2015.2437974.

[7] M. Valavi and A. Nysveen, "Variable-speed operation of hydropower plants: A look at the past, present, and future," *IEEE Ind. Appl. Mag.*, vol. 24, no. 5, pp. 18–27, Sep./Oct. 2018, doi: 10.1109/MIAS.2017.2740467.

[8] R. Kerkman, T. Lipo, W. Newman, and J. Thirkell, "An inquiry into adjustable speed operation of a pumped hydro plant Part 1 - Machine design and performance," *IEEE Trans. Power App. Syst.*, vol. PAS-99, no. 5, pp. 1828–1837, Sep. 1980, doi: 10.1109/tpas.1980.319773.

[9] J.-M. Henry, F. Maurer, J.-L. Drommi, and T. Sautereau, "Converting to variable speed at a pumped-storage plant," in *Proc. 20th Int. Seminar Hydro Rev.*, 2013. [Online]. Available: https://www.hydroreview.com/companies/converting-to-variable-speed-at-a-pumped-storage-plant/

[10] S. Furuya, T. Taguchi, K. Kusunoki, T. Yanagisawa, T. Kageyama, and T. Kanai, "Successful achievement in a variable speed pumped storage power system at Yagisawa power plant," in *Proc. Conf. Rec. Power Convers. Conf.*, 1993, pp. 603–608, doi: 10.1109/PCCON.1993.264187.

[11] A. Hodder, J.-J. Simond, and A. Schwery, "Double-fed asynchronous motor-generator equipped with a 3-level VSI cascade," in *Proc. 39th IAS Annu. Meeting Conf. Rec. IEEE Ind. Appl. Conf.*, 2004, pp. 2762–2769, doi: 10.1109/IAS.2004.1348865.

[12] S. Aubert, "Power on tap," *ABB Rev.*, vol. 3, pp. 26–31, 2011.

[13] H. Schlunegger, "Pumping efficiency, a 100MW converter for the grimsel 2 pumped storage plant," *ABB Rev.*, vol. 2, pp. 42–47, 2014.

[14] J.-M. Claude, "Performances achieved to the grid by a full power converter used in a variable speed pumped storage plant," *J. Phys., Conf.*, vol. 813, Apr. 2017, Art. no. 012008, doi: 10.1088/1742-6596/813/1/012008.

[15] P. K. Steimer, O. Senturk, S. Aubert, and S. Linder, "Converter-fed synchronous machine for pumped hydro storage plants," in *Proc. IEEE Energy Convers. Congr. Expo.*, 2014, pp. 4561–4567, doi: 10.1109/ECCE.2014.6954025.

[16] M. Soares and E. H. Watanabe, "MMC applied to pumped hydro storage using a differentiable approximation of a square wave as common-mode voltage during low-frequency operation," in *Proc. IEEE 21st Workshop Control Model. Power Electron.*, 2020, pp. 1–8, doi: 10.1109/COMPEL49091.2020.9265759.

[17] M. Basić, M. Utvić, and D. Dujic, "Hybrid modular multilevel converter design and control for variable speed pumped hydro storage plants," *IEEE Access*, vol. 9, pp. 140050–140065, 2021, doi: 10.1109/ACCESS.2021.3118277.

[18] R. Tiwari, R. Nilsen, and A. Nysveen, "Evaluation and comparison between multilevel converters for variable speed operation of pumped storage power plants with full-size converters," in *Proc. IEEE Ind. Appl. Soc. Annu. Meeting*, 2021, pp. 1–8, doi: 10.1109/ias48185.2021.9677283.

[19] F. Kammerer, D. Braeckle, M. Gommeringer, M. Schnarrenberger, and M. Braun, "Operating performance of the modular multilevel matrix converter in drive applications," in *Proc. PCIM Europe Int. Exhib. Conf. Power Electron., Intell. Motion, Renewable Energy Energy Manage.*, 2015, pp. 1–8.

[20] D. Weiss, M. Vasiladiotis, C. Banceanu, N. Drack, B. Odegard, and A. Grondona, "IGCT based modular multilevel converter for an AC-AC rail power supply," in *Proc. Int. Exhib. Conf. Power Electron., Intell. Motion, Renewable Energy Energy Manage.*, 2017, pp. 1–8.

[21] T. Thurnherr, P. Maibach, B. Buchmann, and E. Baerlocher, "Static frequency converters for railway power supply based on IGCT high power semiconductors," in *Proc. PCIM Europe Digit. days Int. Exhib. Conf. Power Electron., Intell. Motion, Renewable Energy Energy Manage.*, 2020, pp. 1–8.

[22] M. Vasiladiotis, R. Baumann, C. Häderli, and J. Steinke, "IGCT-Based direct AC/AC modular multilevel converters for pumped hydro storage plants," in *Proc. IEEE Energy Convers. Congr. Expo.*, 2018, pp. 4837–4844, doi: 10.1109/ECCE.2018.8557594.

[23] C. Haederli, T. Thurnherr, A. Christe, A. Faulstich, and C. Ladreiter-Knauss, "Project malta upper stage–world's first direct modular multilevel converter for variable-speed pumped storage hydropower," in *Proc. HYDRO*, 2022.

[24] B. Ødegård, D. Weiss, T. Wikström, and R. Baumann, "Rugged MMC converter cell for high power applications," in *Proc. 18th Eur. Conf. Power Electron. Appl.*, 2016, pp. 1–10, doi: 10.1109/EPE.2016.7695417.

[25] A. J. Korn, M. Winkelnkemper, P. Steimer, and J. W. Kolar, "Direct modular multi-level converter for gearless low-speed drives," in *Proc. 14th Eur. Conf. Power Electron. Appl.*, 2011, pp. 1–7.

[26] W. Kawamura, Y. Chiba, M. Hagiwara, and H. Akagi, "Experimental verification of an electrical drive fed by a modular multilevel TSBC converter when the motor frequency gets closer or equal to the supply frequency," *IEEE Trans. Ind. Appl.*, vol. 53, no. 3, pp. 2297–2306, May/Jun. 2017, doi: 10.1109/TIA.2017.2665635.

[27] B. Fan, K. Wang, P. Wheeler, C. Gu, and Y. Li, "A branch current reallocation based energy balancing strategy for the modular multilevel matrix converter operating around equal frequency," *IEEE Trans. Power Electron.*, vol. 33, no. 2, pp. 1105–1117, Feb. 2018, doi: 10.1109/TPEL.2017.2685431.

[28] M. Depenbrock, "Pulse width control of a 3-phase inverter with non-sinusoidal phase voltages," in *Proc. IEEE Ind. Appl. Soc. Int. Semicond. Power Converter Conf.*, 1977, pp. 399–403.

[29] F. Kammerer, J. Kolb, and M. Braun, "Fully decoupled current control and energy balancing of the modular multilevel matrix converter," in *Proc. 15th Int. Power Electron. Motion Control Conf.*, 2012, pp. LS2a.3–1LS2a.38, doi: 10.1109/EPEPEMC.2012.6397408.
[30] W. Kawamura, M. Hagiwara, and H. Akagi, "Control and experiment of a modular multilevel cascade converter based on triple-star bridge cells," *IEEE Trans. Ind. Appl.*, vol. 50, no. 5, pp. 3536–3548, Sep./Oct. 2014, doi: 10.1109/TIA.2014.2311759.
[31] D. Karwatzki, L. Baruschka, J. Kucka, and A. Mertens, "Current control and branch energy balancing of the modular multilevel matrix converter," in *Proc. IEEE Energy Convers. Congr. Expo.*, 2015, pp. 6360–6367, doi: 10.1109/ECCE.2015.7310551.
[32] A. J. Korn, M. Winkelnkemper, and P. Steimer, "Low output frequency operation of the modular multi-level converter," in *Proc. IEEE Energy Convers. Congr. Expo.*, 2010, pp. 3993–3997, doi: 10.1109/ECCE.2010.5617802.
[33] H. Fujita, S. Tominaga, and H. Akagi, "Analysis and design of a DC voltage-controlled static VAr compensator using quad-series voltage-source inverters," *IEEE Trans. Ind. Appl.*, vol. 32, no. 4, pp. 970–978, Jul./Aug. 1996, doi: 10.1109/28.511656.
[34] T. Holzer, A. Muetze, G. Traxler-Samek, M. Lecker, and F. Zerobin, "Generator design possibilities for full-size converter operation of large pumped storage power plants," *IEEE Trans. Ind. Appl.*, vol. 56, no. 4, pp. 3644–3655, Jul./Aug. 2020, doi: 10.1109/TIA.2020.2989074.
[35] F. Kammerer, M. Gommeringer, J. Kolb, and M. Braun, "Energy balancing of the modular multilevel matrix converter based on a new transformed arm power analysis," in *Proc. 16th Eur. Conf. Power Electron. Appl.*, 2014, pp. 1–10, doi: 10.1109/EPE.2014.6910939.
[36] A. Yazdani and R. Iravani, *Voltage-Sourced Converters in Power Systems: Modeling, Control, and Applications*. Hoboken, NJ, USA: Wiley-IEEE Press, 2010.
[37] K. Hasse, "Zur dynamik drehzahlgeregelter antriebe mit stromrichtergespeisten asynchron-kurzschlussläufermaschinen," Ph.D. dissertation, Technische Universität Darmstadt, 1969.
[38] F. Blaschke, "Das verfahren der feldorientierung zur regelung der drehfeldmaschine," Ph.D. dissertation, Technische Universitsät Braunschweig, 1973.
[39] *E-Control. TOR Erzeuger Typ D*. Dec. 2019. [Online]. Available: https://www.e-control.at/documents/1785851/1811582/TORErzeugerTypDV1.0.pdf/ae8394df-60aa-5a4f-738e-a6df14a72541?t=1562757862259
[40] N. Patzelt, C. Schlegel, and M. Vasiladiotis, "Multi-objective optimization of modular multilevel converter systems," in *Proc. 24th Eur. Conf. Power Electron. Appl.*, 2022.
[41] C. Nicolet, O. Braun, N. Ruchonnet, A. Béguin, and F. Avellan, "Full size frequency converter for fast francis pump-turbine operating mode transition," in *Proceedings of HYDROVISION International*, Minneapolis, MN, USA: Minneapolis Convention Center, Jul. 26-29, 2016.

Alexandre Christe (Member, IEEE) received the BSc. and MSc. degrees in electrical engineering and the Ph.D. degree in energy from École Polytechnique Fédérale de Lausanne, Switzerland, in 2012, 2014, and 2018, respectively.

From April 2014 to March 2018, he was a Doctoral Assistant with the Power Electronics Laboratory. From May 2018 to August 2019, he was a Scientist with ABB Corporate Research Center, Västerås, Sweden. Since August 2019, he is with (now called) Hitachi Energy, Turgi, Switzerland, where he is currently a Senior R&D Engineer working on the product development of medium-voltage high-power multilevel static frequency converters, in particular for pumped storage hydropower.

Alexander Faulstich received the Dipl.-Ing. degree in electrical engineering with focus on automation from Technische Universität Dresden, Germany, in 1996.

He joined ABB (now Hitachi Energy) in Turgi, Switzerland, in 1998, where he is currently a Senior R&D Engineer working on the product development of medium-voltage converters. He is involved in the closed-loop control development, integration, testing, and commissioning.

Michail Vasiladiotis (Senior Member, IEEE) received the Diploma in electrical and computer engineering from the National Technical University of Athens, Athens, Greece, in 2009, and the Ph.D. degree in energy from École Polytechnique Fédérale de Lausanne, Lausanne, Switzerland, in 2014.

Since 2015, he has been with Hitachi Energy (former ABB), Turgi, Switzerland, where he is currently leading the R&D team for power conversion. He is the author/co-author of several journal articles, conference papers and patent applications.

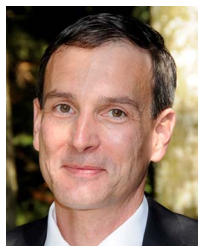

Peter Steinmann received the Bachelor of Science degree in electrical engineering from Zentralschweizerisches Technikum Luzern, Germany, in 1991.

He joined ABB (now Hitachi Energy) in Turgi, Switzerland, in 1992, where he is currently a Principal Engineer working for project execution focusing on control protection and commissioning.